Hemodynamics in coronary arteries with overlapping stents

Rikhtegar, Farhad ; Wyss, Christophe ; Stok, Kathryn S ; Poulikakos, Dimos ; Müller, Ralph ; Kurtcuoglu, Vartan

Abstract: Coronary artery stenosis is commonly treated by stent placement via percutaneous intervention, at times requiring multiple stents that may overlap. Stent overlap is associated with increased risk of adverse clinical outcome. While changes in local blood flow are suspected to play a role therein, hemodynamics in arteries with overlapping stents remain poorly understood. In this study we analyzed six cases of partially overlapping stents, placed ex vivo in porcine left coronary arteries and compared them to five cases with two non-overlapping stents. The stented vessel geometries were obtained by micro-computed tomography of corrosion casts. Flow and shear stress distribution were calculated using computational fluid dynamics. We observed a significant increase in the relative area exposed to low wall shear stress (WSS<0.5Pa) in the overlapping stent segments compared both to areas without overlap in the same samples, as well as to non-overlapping stents. We further observed that the configuration of the overlapping stent struts relative to each other influenced the size of the low WSS area: positioning of the struts in the same axial location led to larger areas of low WSS compared to alternating struts. Our results indicate that the overlap geometry is by itself sufficient to cause unfavorable flow conditions that may worsen clinical outcome. While stent overlap cannot always be avoided, improved deployment strategies or stent designs could reduce the low WSS burden.

DOI: https://doi.org/10.1016/j.jbiomech.2013.10.048

Hemodynamics in coronary arteries with overlapping stents

Farhad Rikhtegar[a], Christophe Wyss[b], Kathryn S. Stok[c], Dimos Poulikakos[a], Ralph Müller[c], Vartan Kurtcuoglu[a,d]

[a] Laboratory of Thermodynamics in Emerging Technologies, Department of Mechanical and Process Engineering, ETH Zurich, Zurich, Switzerland
[b] Clinic of Cardiology, University Hospital Zurich, Zurich, Switzerland
[c] Institute for Biomechanics, Department Health Sciences and Technology, ETH Zurich, Zurich, Switzerland
[d] The Interface Group, Institute of Physiology, University of Zurich, Zurich, Switzerland

Corresponding Author:
Vartan Kurtcuoglu
Winterthurerstr. 190, Y23 J8
8057 Zurich, Switzerland
E-mail: vartan.kurtcuoglu@uzh.ch
Phone: +41 44 635 50 55
Fax: +41 44 635 68 14

Abstract

Coronary artery stenosis is commonly treated by stent placement via percutaneous intervention, at times requiring multiple stents that may overlap. Stent overlap is associated with increased risk of adverse clinical outcome. While changes in local blood flow are suspected to play a role therein, hemodynamics in arteries with overlapping stents remain poorly understood. In this study we analyzed six cases of partially overlapping stents, placed ex vivo in porcine left coronary arteries and compared them to five cases with two non-overlapping stents. The stented vessel geometries were obtained by micro-computed tomography of corrosion casts. Flow and shear stress distribution were calculated using computational fluid dynamics. We observed a significant increase in the relative area exposed to low wall shear stress (WSS < 0.5 Pa) in the overlapping stent segments compared both to areas without overlap in the same samples, as well as to non-overlapping stents. We further observed that the configuration of the overlapping stent struts relative to each other influenced the size of the low WSS area: Positioning of the struts in the same axial location led to larger areas of low WSS compared to alternating struts. Our results indicate that the overlap geometry is by itself sufficient to cause unfavorable flow conditions that may worsen clinical outcome. While stent overlap cannot always be avoided, improved deployment strategies or stent designs could reduce the low WSS burden.

Keywords:

- Stent overlap
- Thrombosis
- Hemodynamics
- Wall shear stress
- Restenosis

1. Introduction

About 30% of patients undergoing percutaneous coronary intervention (PCI) with stent placement are treated with overlapping stents (Holmes et al., 2004; Räber et al., 2010). Stent overlap is associated with increased risk of adverse clinical outcome for both bare metal stents (BMS) and drug eluting stents (DES) (Ellis et al., 1992; Räber et al., 2010). Various studies have investigated clinical results and biological aspects of stent overlap, but the hemodynamics inside arteries with overlapping stents and the associated wall shear stress (WSS) parameters have received much less attention (Balakrishnan et al., 2005; Charonko et al., 2010; Peacock et al., 1995). This can be in part attributed to the lack of suitable methods for acquiring the geometry of arteries containing overlapping stents with sufficient accuracy.

Stent overlap is associated with increased in-stent restenosis and lumen loss due to delayed healing and increased inflammation regardless of stent type (Räber et al., 2010; Wang et al., 2000). While DES may reduce neointimal hyperplasia and restenosis in single stent cases (Moses et al., 2003; Tsagalou et al., 2005), their performance (Finn et al., 2005; Matsumoto et al., 2007) and safety (Moreno et al., 2005) in regions of overlap are a case of debate. Overlapping BMS are associated with worse clinical outcome compared to single BMS (Kastrati et al., 1999; Kereiakes et al., 2006; Serruys et al., 2002). This is attributed primarily to more pronounced arterial injury caused by the expansion of two stents at the same location, leading to increased inflammation. However, the poorer outcome may also be related to severe hemodynamic disturbances introduced by stent malapposition (Charonko et al., 2010) that are inherent in stent overlap but occur infrequently in single stents (Matsumoto et al., 2007).

It is generally accepted that hemodynamics influences vascular health and pathogenesis. WSS as one of the manifestations of blood flow has been shown to be an important factor in atherogenesis (Chatzizisis et al., 2007; Cheng et al., 2006) and in the pathobiology of neointimal hyperplasia, thrombosis and in-stent restenosis (Papafaklis et al., 2010; Wentzel et al., 2008). These latter processes are a concern in percutaneous vascular intervention in general and in stent placement in particular. For example, stent malapposition has been shown to increase thrombogenicity. It is

hypothesized that hemodynamics play a role therein, as adjacent high shear stress areas and recirculation zones caused by malapposed stents may activate platelets and increase local residence times of these thrombocytes (Hathcock, 2006; Kolandaivelu et al., 2011; Peacock et al., 1995). Kolandaivelu and co-workers showed in vitro and in a 2D computational model with idealized domain geometry that flow recirculation between malapposed and overlapping stent struts may modulate stent thrombogenicity (Kolandaivelu et al., 2011).

Computational fluid dynamics (CFD) is the method of choice for assessing shear stress and local hemodynamics in stented arteries. The precise acquisition of the stent struts and arterial geometry is a prerequisite for accurate CFD analysis, but no clinical imaging modality exists that could yield such data with sufficient resolution. Several approaches have been reported in the literature to circumvent this limitation: Simulations may be conducted on idealized geometries based on stent CAD data (Gundert et al., 2011), on hybrid domains where the stent free geometry is obtained by CT, digital angiography or MRI and a stent is virtually implanted (De Santis et al., 2010; LaDisa et al., 2006), on ex vivo micro-computed tomography (μCT) data of explanted, stented arteries (Morlacchi et al., 2011) or μCT images of stented in vitro artery models (Benndorf et al., 2009; Connolley et al., 2007). While these methods have their undisputed respective strengths, they have either limited geometric accuracy, limited treatable vascular domain size or incomplete representation of the mechanical interaction between stent and arterial wall.

We have recently introduced a method that allows for precise ex vivo acquisition of arteries stented in vivo or ex vivo, yielding both the macroscopic arterial tree geometry as well as the configuration and morphology of individual stent struts (Rikhtegar et al., 2013). Here we make use of this method to investigate the shear stress distribution and hemodynamics of porcine coronary arteries with overlapping stents. Our goal is to evaluate flow disturbances and consequent shear stress alterations introduced by stent overlap which may contribute to the reported clinical problems associated with overlapping stents.

2. Methods

A concise description of the utilized methods is given here. We refer the reader to the supplemental material and (Rikhtegar et al., 2013) for a more detailed explanation of the individual process steps.

2.1. Heart preparation, stenting and vascular corrosion casting

After cannulation, two absorbable metal scaffolds of 10 mm length and 3 mm diameter (Biotronik AG, Switzerland) were implanted in the left coronary artery of eleven ex vivo porcine hearts under angiographic guidance by an interventional cardiologist. The scaffolds had overlap in six arteries. The remaining five arteries served as control (no overlap).

A radio-opaque casting material was prepared as a mixture of Biodur E20 resin (Biodur Products GmbH, Germany) and iodine-saturated methyl ethyl ketone solvent. The casting material was injected into the stented arteries under physiological pressure of 90 mmHg. The hearts were left at room temperature for 36 hours, and then macerated at 55 °C in a 7.5% w/v solution of potassium hydroxide. The final products were rinsed with water to remove remaining tissue.

2.2. μCT imaging of stented casts and image processing

Micro-computed tomography (μCT80, Scanco Medical AG, Switzerland) was used with an isotropic voxel size of 74 μm (energy 70kVp, integration time 300 ms, tube current 114 μA, and two times frame averaging) to capture the overall geometry of the arterial tree. The stented vessel segments were dissected from the remainder of the arterial tree and re-scanned at higher resolution (μCT40, Scanco) with an isotropic voxel size of 6 μm (energy 70kVp, integration time 300 ms, tube current 114 μA, and two times frame averaging).

To partly suppress noise in the raw μCT volumes, a constrained 3D Gauss filter was used ($\sigma = 1.2$, support = 1). Both μCT datasets of low and high resolution were independently segmented using a semi-automatic, intensity-based approach in Avizo 6.2 (Visualization Sciences Group SAS, France) to obtain the lumen geometry. The resulting 3D geometries were exported to Geomagic Studio 12 (Geomagic, Inc., USA) to register and merge the high resolution geometry of the stented segment and the low resolution remainder of the arterial tree.

2.3. CFD calculations

ANSYS ICEM CFD (ANSYS, Inc., USA) was used to generate a computational grid consisting of approximately 50 million tetrahedral elements in the merged geometry. Steady-state CFD analysis was carried out with the finite volume code ANSYS CFX to determine hemodynamics and WSS distribution. Blood was modeled as a non-Newtonian fluid with constant density of 1050 kg/m^3 and shear dependent dynamic viscosity according to the Carreau model (Chien et al., 1966). Inflow rate was set to 0.95 mL/s at the coronary ostium (Berne, 1986) and no slip was prescribed at the stent surfaces and vessel wall. Murray's law was applied at the outlets to where the largest diameter branch had zero relative pressure. Outflow rates at the remaining outlets were determined according to their cross-sectional area (Murray, 1926; Rikhtegar et al., 2013). Residual reduction to 10^{-8} of the initial value was set as the convergence criterion. Grid independence studies confirmed that the chosen grid was sufficient to capture WSS with a relative error of <4% compared to a grid with 100% higher cell density.

3. Results

It has been shown previously that the acquisition method used here can capture single stented arteries accurately at high resolution (Rikhtegar et al., 2013). Fig. 1 illustrates that this method also ensures anatomic fidelity in the case of overlapping stents, showing that it captures regions of prolapse between stent struts (Panel A), axial arterial deformation caused by the stent implantation (Panel B), strut overlap and relative positioning (Panel C), radial arterial deformation (Panel D) and strut malapposition (Panel E).

WSS distribution in one of the porcine left coronary arteries with overlapping stents is shown in Fig. 2. Here as in subsequent figures, reported WSS values are normalized with respect to the maximum WSS along the arterial tree, which ranges between 9.5 and 11 Pa depending on the investigated case. Absolute values are given in the supplemental material. Shear stress below 5% of the maximum WSS is shown in dark blue. This corresponds to approximately 0.5 Pa, here referred to as low and atheroprone according to (Garasic et al., 2000). Such low WSS is present around individual stent struts and at bifurcations. It is clearly visible in the inset that a larger wall area is exposed to low shear stress

161 in the overlapped region compared to the adjacent areas covered by a single stent. This is not an
162 observation that is limited to one sample: All six overlapping stents demonstrate the same qualitative
163 behavior (Fig. 3). Differences between the six cases are mostly due to varying stent overlap length:
164 Samples I-III have clearly shorter overlap regions compared to the other cases, resulting in smaller
165 areas of low WSS.

166 To understand why larger wall areas are exposed to low WSS in the overlapping stent segments, local
167 hemodynamics must be considered. Fig. 4 shows streamlines projected onto an axial cut plane in the
168 vicinity of stent struts. Panel A illustrates the velocity pattern in an overlap segment where blood is
169 tunneled between two alternating struts. Recirculation zones are visible adjacent to the outer stent
170 struts. A large recirculation zone between two struts in close vicinity is shown in panel B. This
171 configuration can occur in stent overlap zones, yielding increased local blood residence times and
172 decreased WSS. Such recirculation zones inherently yield low WSS values.

173 The struts of overlapping stents can either be aligned (the inner stent's struts are located immediately
174 on top of the outer struts), or positioned in an alternating fashion (the struts of the stents are axially
175 offset). We refer to these as congruent and incongruent strut configurations, respectively. Differences
176 in the flow field between congruent and incongruent configurations are presented in Fig. 5. Velocity
177 magnitudes are higher near the wall in the incongruent case, where blood can flow between the
178 alternating struts (compare Fig. 6). In contrast, the congruent strut configuration produces larger
179 obstacles to flow, increasing recirculation zone sizes. The relative positioning of the overlapping-stent
180 struts influence the location of the stagnation points and alter the extent of recirculation zones
181 compared to struts without overlap.

182 The effect of strut alignment on WSS distribution is shown in Fig. 6, where a longitudinal cut of
183 stented segment is overlaid by WSS contour. Congruent strut regions (black arrows) feature lower
184 WSS compared to areas with alternating struts (white arrows), where the blood can flow at higher
185 velocity near the vessel wall.

186 Fig. 7 shows normalized WSS along two axial paths past a set of representative congruent and
187 incongruent struts, respectively. With the exception of the actual strut wall, WSS is lower in the

congruent configuration. The higher WSS at the strut wall is caused by tunneling of blood between the closely-spaced congruent struts at increased speed. Normalized flow speeds between pairs of adjacent stent struts in congruent and incongruent cases are plotted in Fig. 8. Lower speeds are observed between pairs of congruent struts due to the formation of larger recirculation zones. It should be noted that this finding cannot be generalized to all strut pairs. The three-dimensional nature of the flow field may counteract the formation of large recirculation zones in the congruent strut configuration or promote formation of such in the incongruent configuration.

To further quantify the observed phenomena, we compared six cases of arteries with overlapping stents to five arteries with two non-overlapping stents. We chose low WSS (<5% of maximum WSS) as the relevant parameter, since it plays a critical role in the biological response of arteries to stent deployment. In the cases with overlap (OV), the overlapping segments as well as the segments proximal and distal to the overlap were evaluated (Fig. 9). In the non-overlap cases (NO), the proximal and distal stents were considered. Since the segment lengths are not all equal, the total area of low WSS was normalized by the respective segment's length.

Over the whole stented artery length, the OV cases show a normalized area of low WSS equal to 7.7 mm^2/mm, which is 57% higher than in the combined segments of the NO cases. Qualitatively similar results were obtained when comparing the area exposed to low WSS in proximal and distal NO stent segments to the proximal and distal segments of the OV cases, respectively: The OV cases showed on average approximately 35% higher values of normalized area exposed to low WSS. Comparison of the overlap segment alone to the combined NO segments and to the combined remaining non-overlap segments of the OV cases showed approximately 102% and 29% higher normalized area of low WSS values, respectively.

4. Discussion

It is known that hemodynamics influences atherogenesis (Chatzizisis et al., 2007; Samady et al., 2011), thrombogenesis (Hathcock, 2006), vascular remodeling (Stone et al., 2003), neointimal hyperplasia (Wentzel et al., 2001) and endothelial healing (Franco et al., 2013). It is further known that stent overlap, compared to single stents, increases thrombogenicity (Kolandaivelu et al., 2011; Rogers

215 and Edelman, 1995), may delay the re-endothelization and enhance platelet deposition and thrombus
216 formation (Finn et al., 2005; Murasato et al., 2010). Poor re-endothelization, in turn, can lead to
217 chronic inflammation (Matsumoto et al., 2007), late stent thrombosis (Moreno et al., 2005) and
218 increased late lumen loss (Räber et al., 2010). Despite the documented importance of hemodynamic
219 factors on vascular biology and outcome of intervention, the effect of overlapping stents on
220 hemodynamics remains poorly understood. In this study we have investigated in a realistic domain
221 flow and shear stress conditions in coronary arteries with overlapping stents.
222 While approaches similar to the one presented here have been used to study hemodynamics in stented
223 arteries, this is, to our knowledge, the first anatomically accurate comprehensive computational
224 analysis of blood flow in overlapping stents. A cross-validation and quantitative comparison of results
225 is thus not possible. However, the reported WSS values are comparable in range to those published for
226 single stents (LaDisa et al., 2005; Benndorf et al., 2010; Morlacchi et al., 2011), and regions of low,
227 atheroprone shear stress are present at bifurcations (Goubergrits et al., 2008; Williams et al., 2010) and
228 nearby individual stent struts (Gundert et al., 2011; Balossino et al., 2008; Charonko et al., 2010).

229 Our results show that areas of low WSS relative to stent size are significantly increased in overlapping
230 stents compared to non-overlapping stents. This is, for one, due to the enlargement of recirculation
231 zones caused by stent strut overlap (Fig. 2). This effect is independent of whether the stent eludes
232 drugs or not, but it is dependent on stent design. Increased low WSS areas, which can be seen in Fig.
233 3, may delay re-endothelization and wall healing, thereby promoting platelet deposition and thrombus
234 formation (Finn et al., 2005; Matsumoto et al., 2007; Murasato et al., 2010). The latter two are either
235 an effect of or compounded by locally increased blood residence times caused by the recirculation
236 zone.

237 It may not be intuitively clear why in the comparison of the proximal and distal segments the OV
238 cases showed larger normalized areas exposed to low WSS than the NO cases. This can be explained,
239 for one, by the fact that the overlapping struts not only affect the flow field in the overlap segment, but
240 also alter flow proximally and distally: The overlapping struts act as taller obstacles, deflecting the
241 flow from the wall, thereby reducing near-wall velocity and increasing the size of recirculation zones,
242 which lead to larger areas of low WSS. Additionally, the here utilized metric of low WSS per unit

stent segment length favors longer segments, where the relative size of the low WSS prone stent end regions is smaller.

Another factor influencing hemodynamics is stent malapposition (Figs. 4 and 5), which also occurs at times in non-overlapping stents (van Geuns et al., 2012) , but it is inherent in overlapping stents (Guagliumi et al., 2010). This is a result of the outer stent blocking the inner from fully contacting the vessel wall, as shown in Fig.1, panels B and C, where the stent rendered in red is not apposed to the wall in the overlap segment. Malapposition of stent struts also leads to alterations in WSS profile (Fig. 6 and 7). The type of influence on hemodynamics and shear stress depends on the stent strut configuration. When the struts of the overlapping stents are placed directly on top of each other (congruent configuration, Fig. 5 bottom), a larger obstacle to blood flow is generated near the vessel wall that resembles a single thick strut. Thick stent struts have been shown to result in increased rates of restenosis and thrombosis due to larger regions of recirculation and flow separation (Kastrati et al., 2001; Kolandaivelu et al., 2011; Pache et al., 2003; Rogers and Edelman, 1995). When struts are not aligned (incongruent configuration, Fig. 5 top), the near-wall blood flow velocity is not reduced to the extent observed in the congruent configuration, as blood is tunneled between the alternating struts. Similarly, WSS values are also not reduced as much as in the congruent setup (Fig. 6 and 8), but spatial WSS gradients are increased. While it has been speculated that high spatial WSS gradients may promote atherosclerosis (Wells et al., 1996), this could not be confirmed to date (Chen et al., 2011; Knight et al., 2010; Rikhtegar et al., 2012). The incongruent configuration should thus be considered superior to the congruent one. That said, novel tools are required to purposefully obtain congruent configurations in clinical practice.

The observed hemodynamic effects result in increased relative areas of low WSS in the stent overlap region compared to the proximal and distal non-overlap segments (Fig. 9). The relative low WSS area is also increased in size with respect to segments of two separate non-overlapping stents. These results are independent of the general stent type (BMS or DES), as the overlap geometry causes unfavorable flow conditions that may worsen clinical outcome (e.g. as quantified by the rate of stent thrombosis and in-stent restenosis) compared to non-overlapping stents. While stent overlap cannot always be

avoided, improved deployment strategies or stent designs could be developed to obtain as much as possible incongruent strut configurations in the area of stent overlap.

4.1. Study Limitations

Choosing proper boundary conditions is important for the correct calculation of WSS distribution (van der Giessen et al., 2011). Here we have used a generic volumetric inflow rate and Murray's law to set the outlet boundary conditions. Subject-specific measurements for in- and out-flow conditions could yield more precise results. This would entail utilizing different imaging modalities such as phase contrast magnetic resonance imaging, invasive intravascular Doppler ultrasound or in vivo flow or pressure measurements that come with their own limitations (Johnson et al., 2008).

Stenting was carried out in partially deflated hearts that contained saline solution in the atria and ventricles. Casting and curing of the resin took place with the hearts submerged under water with filled atria and ventricles, and arteries pressurized to a physiologic level. Ideally, physiologic pressure levels would be maintained in all compartments throughout the procedure, which may give a more accurate representation of the arterial geometry. This would, however, also substantially increase the experiment's complexity.

The biological response of the vascular wall is not considered here, and merely hemodynamic effects were investigated. Incorporating more complex models that take into account vascular biology and transport processes (Olgac et al., 2011) would give deeper insight into the topic, as would the inclusion of a wall injury model. The latter is relevant due to the increased mechanical load in areas of stent overlap.

Hemodynamics also influence the distribution and uptake of drugs eluted from DES, which in turn affect endothelial healing, stent thrombosis and in-stent restenosis. In this study, we have not distinguished between BMS and DES, but considered exclusively the common effect of hemodynamics. Since DES are steadily replacing BMS in clinical practice, it will be important to quantify the effect of flow on local drug concentration.

5. Conclusion

We have shown that the relative size of low WSS areas is increased significantly in regions of stent overlap compared to non-overlapped regions. Since low WSS is generally accepted as a factor in atherogenesis and thrombogenesis, we conclude that the adverse hemodynamics caused by stent overlap may be responsible in part for the adverse clinical outcome in patients that are treated with overlapping stents. In cases where stent overlap cannot be avoided, new deployment strategies or stent designs should be considered to reduce the size of low WSS areas.

Acknowledgments

We thank Ryan J. Choo and Gian N. Schädli of ETH Zurich for help with the micro-computed tomography and image segmentation, respectively. This work was partially funded by the Swiss Federal Commission for Technology and Innovation through EnOp, grant 9921.1, and the Swiss National Science Foundation through NCCR Kidney.CH.

Conflict of interest statement

We have no conflicts of interest to report.

6. References

Balakrishnan, B., Tzafriri, A.R., Seifert, P., Groothuis, A., Rogers, C., Edelman, E.R., 2005. Strut Position, Blood Flow, and Drug Deposition: Implications for Single and Overlapping Drug-Eluting Stents. Circulation 111, 2958-2965.

Balossino, R., Gervaso, F., Migliavacca, F., Dubini, G., 2008. Effects of different stent designs on local hemodynamics in stented arteries. Journal of Biomechanics 41, 1053-1061.

Benndorf, G., Ionescu, M., Y Alvarado, M.V., Biondi A., Hipp J., Metcalfe, R., 2010. Anomalous hemodynamic effects of a self-expanding intracranial stent: comparing in-vitro and ex-vivo models using ultra-high resolution microCT based CFD. Journal of biomechanics 43, 740-748.

Benndorf, G., Ionescu, M., Y Alvarado, M.V., Hipp, J., Metcalfe, R., 2009. Wall Shear Stress in Intracranial Self-Expanding Stents Studied Using Ultra-High-Resolution 3D Reconstructions. American Journal of Neuroradiology 30, 479-486.

Berne, R.M., Levy, M.N., 1986. Cardiovascular Physiology 5th ed. Mosby, St. Louis.

Charonko, J., Karri, S., Schmieg, J., Prabhu, S., Vlachos, P., 2010. In vitro comparison of the effect of stent configuration on wall shear stress using time-resolved particle image velocimetry. Annals of Biomedical Engineering 38, 889-902.

Chatzizisis, Y.S., Coskun, A.U., Jonas, M., Edelman, E.R., Feldman, C.L., Stone, P.H., 2007. Role of Endothelial Shear Stress in the Natural History of Coronary Atherosclerosis and Vascular Remodeling: Molecular, Cellular, and Vascular Behavior. Journal of the American College of Cardiology 49, 2379-2393.

Chen, H.Y., Sinha, A.K., Choy, J.S., Zheng, H., Sturek, M., Bigelow, B., Bhatt, D.L., Kassab, G.S., 2011. Mis-sizing of stent promotes intimal hyperplasia: impact of endothelial shear and intramural stress. American Journal of Physiology - Heart and Circulatory Physiology 301, H2254-H2263.

Cheng, C., Tempel, D., van Haperen, R., van der Baan, A., Grosveld, F., Daemen, M.J.A.P., Krams, R., de Crom, R., 2006. Atherosclerotic Lesion Size and Vulnerability Are Determined by Patterns of Fluid Shear Stress. Circulation 113, 2744-2753.

Chien, S., Usami, S., Taylor, H.M., Lundberg, J.L., Gregerse.Mi, 1966. Effects of hematocrit and plasma proteins on human blood rheology at low shear rates. Journal of Applied Physiology 21, 81-87.

Connolley, T., Nash, D., Buffière, J.-Y., Sharif, F., McHugh, P.E., 2007. X-ray micro-tomography of a coronary stent deployed in a model artery. Medical Engineering & Physics 29, 1132-1141.

De Santis, G., Mortier, P., De Beule, M., Segers, P., Verdonck, P., Verhegghe, B., 2010. Patient-specific computational fluid dynamics: structured mesh generation from coronary angiography. Medical & Biological Engineering & Computing 48, 371-380.

Ellis, S.G., Savage, M., Fischman, D., Baim, D.S., Leon, M., Goldberg, S., Hirshfeld, J.W., Cleman, M.W., Teirstein, P.S., Walker, C., Bailey, S., Buchbinder, M., Topol, E.J., Schatz, R.A., 1992. Restenosis after placement of Palmaz-Schatz stents in native coronary arteries. Initial results of a multicenter experience. Circulation 86, 1836-1844.

Finn, A.V., Kolodgie, F.D., Harnek, J., Guerrero, L.J., Acampado, E., Tefera, K., Skorija, K., Weber, D.K., Gold, H.K., Virmani, R., 2005. Differential Response of Delayed Healing and Persistent Inflammation at Sites of Overlapping Sirolimus- or Paclitaxel-Eluting Stents. Circulation 112, 270-278.

Franco, D., Milde, F., Klingauf, M., Orsenigo, F., Dejana, E., Poulikakos, D., Cecchini, M., Koumoutsakos, P., Ferrari, A., Kurtcuoglu, V., 2013. Accelerated endothelial wound healing on microstructured substrates under flow. Biomaterials 34, 1488-1497.

Garasic, J.M., Edelman, E.R., Squire, J.C., Seifert, P., Williams, M.S., Rogers, C., 2000. Stent and artery geometry determine intimal thickening independent of arterial injury. Circulation 101, 812-818.

Goubergrits, L., Kertzscher, U., Schöneberg, B., Wellnhofer, E., Petz, C., Hege, H.-C., 2008. CFD analysis in an anatomically realistic coronary artery model based on non-invasive 3D imaging: comparison of magnetic resonance imaging with computed tomography. International Journal of Cardiovascular Imaging 24, 411-421.

Guagliumi, G., Musumeci, G., Sirbu, V., Bezerra, H.G., Suzuki, N., Fiocca, L., Matiashvili, A., Lortkipanidze, N., Trivisonno, A., Valsecchi, O., Biondi-Zoccai, G., Costa, M.A., Investigators, O.T., 2010. Optical Coherence Tomography Assessment of In Vivo Vascular Response After Implantation of Overlapping Bare-Metal and Drug-Eluting Stents. Journal of the American College of Cardiology-Cardiovascular Interventions 3, 531-539.

Gundert, T., Shadden, S., Williams, A., Koo, B.-K., Feinstein, J., LaDisa, J., 2011. A Rapid and Computationally Inexpensive Method to Virtually Implant Current and Next-Generation Stents into Subject-Specific Computational Fluid Dynamics Models. Annals of Biomedical Engineering 39, 1423-1437.

Hathcock, J.J., 2006. Flow Effects on Coagulation and Thrombosis. Arteriosclerosis, Thrombosis, and Vascular Biology 26, 1729-1737.

Holmes, D.R., Leon, M.B., Moses, J.W., Popma, J.J., Cutlip, D., Fitzgerald, P.J., Brown, C., Fischell, T., Wong, S.C., Midei, M., Snead, D., Kuntz, R.E., 2004. Analysis of 1-Year Clinical Outcomes in the SIRIUS Trial: A Randomized Trial of a Sirolimus-Eluting Stent Versus a Standard Stent in Patients at High Risk for Coronary Restenosis. Circulation 109, 634-640.

Johnson, K., Sharma, P., Oshinski, J., 2008. Coronary artery flow measurement using navigator echo gated phase contrast magnetic resonance velocity mapping at 3.0 Tesla. Journal of Biomechanics 41, 595-602.

Kastrati, A., Elezi, S., Dirschinger, J., Hadamitzky, M., Neumann, F.J., Schomig, A., 1999. Influence of lesion length on restenosis after coronary stent placement. Ameican Journal of Cardiology 83, 1617-1622.

Kastrati, A., Mehilli, J., Dirschinger, J., Dotzer, F., Schuhlen, H., Neumann, F.J., Fleckenstein, M., Pfafferott, C., Seyfarth, M., Schomig, A., 2001. Intracoronary stenting and angiographic results

- Strut thickness effect on restenosis outcome (ISAR-STEREO) trial. Circulation 103, 2816-2821.

Kereiakes, D.J., Wang, H., Popma, J.J., Kuntz, R.E., Donohoe, D.J., Schofer, J., Schampaert, E., Meier, B., Leon, M.B., Moses, J.W., 2006. Periprocedural and Late Consequences of Overlapping Cypher Sirolimus-Eluting Stents: Pooled Analysis of Five Clinical Trials. Journal of the American College of Cardiology 48, 21-31.

Knight, J., Olgac, U., Saur, S.C., Poulikakos, D., Marshall Jr, W., Cattin, P.C., Alkadhi, H., Kurtcuoglu, V., 2010. Choosing the optimal wall shear parameter for the prediction of plaque location--A patient-specific computational study in human right coronary arteries. Atherosclerosis 211, 445-450.

Kolandaivelu, K., Swaminathan, R., Gibson, W.J., Kolachalama, V.B., Nguyen-Ehrenreich, K.-L., Giddings, V.L., Coleman, L., Wong, G.K., Edelman, E.R., 2011. Stent Thrombogenicity Early in High-Risk Interventional Settings Is Driven by Stent Design and Deployment and Protected by Polymer-Drug Coatings. Circulation 123, 1400-1409.

LaDisa, J.F., Jr., Olson, L., Douglas, H., Warltier, D., Kersten, J., Pagel, P.S., 2006. Alterations in regional vascular geometry produced by theoretical stent implantation influence distributions of wall shear stress: analysis of a curved coronary artery using 3D computational fluid dynamics modeling. Biomedical Engineering Online 5, 40.

LaDisa, J.F., Jr., Olson, L.E., Guler, I, Hettrick, D.A., Kersten, J.R., Warltier, D.C., Pagel, P.S., 2005. Circumferential vascular deformation after stent implantation alters wall shear stress evaluated with time-dependent 3D computational fluid dynamics models. Journal of applied physiology 98, 947-957.

Matsumoto, D., Shite, J., Shinke, T., Otake, H., Tanino, Y., Ogasawara, D., Sawada, T., Paredes, O.L., Hirata, K.-i., Yokoyama, M., 2007. Neointimal coverage of sirolimus-eluting stents at 6-month follow-up: evaluated by optical coherence tomography. European Heart Journal 28, 961-967.

Moreno, R., Fernandez, C., Hernandez, R., Alfonso, F., Angiolillo, D.J., Sabate, M., Escaned, J., Banuelos, C., Fernandez-Ortiz, A., Macaya, C., 2005. Drug-eluting stent thrombosis - Results from a pooled analysis including 10 randomized studies. Journal of the American College of Cardiology 45, 954-959.

Morlacchi, S., Keller, B., Arcangeli, P., Balzan, M., Migliavacca, F., Dubini, G., Gunn, J., Arnold, N., Narracott, A., Evans, D., Lawford, P., 2011. Hemodynamics and in-stent restenosis: micro-CT images, histology, and computer simulations. Annals of Biomedical Engineering 39, 2615-2626.

Moses, J.W., Leon, M.B., Popma, J.J., Fitzgerald, P.J., Holmes, D.R., O'Shaughnessy, C., Caputo, R.P., Kereiakes, D.J., Williams, D.O., Teirstein, P.S., Jaeger, J.L., Kuntz, R.E., 2003. Sirolimus-eluting stents versus standard stents in patients with stenosis in a native coronary artery. The New England journal of medicine 349, 1315-1323.

Murasato, Y., Hikichi, Y., Nakamura, S., Kajiya, F., Iwasaki, K., Kinoshita, Y., Yamawaki, M., Shinke, T., Yamada, S., Yamashita, T., Choo, G.-H., Nam, C.-W., Kim, Y.-H., Jepson, N., Ferenc, M., 2010. Recent Perspective on Coronary Bifurcation Intervention: Statement of the "Bifurcation Club in KOKURA". Journal of Interventional Cardiology 23, 295-304.

Murray, C.D., 1926. The Physiological Principle of Minimum Work. I. The Vascular System and the Cost of Blood Volume. Proceedings of the National Academy of Sciences of the United States of America 12, 207-214.

Olgac, U., Knight, J., Poulikakos, D., Saur, S.C., Alkadhi, H., Desbiolles, L.M., Cattin, P.C., Kurtcuoglu, V., 2011. Computed high concentrations of low-density lipoprotein correlate with plaque locations in human coronary arteries. Journal of Biomechanics 44, 2466-2471.

Pache, J., Kastrati, A., Mehilli, J., Schuhlen, H., Dotzer, F., Hausleiter, J., Fleckenstein, M., Neumann, F.J., Sattelberger, U., Schmitt, C., Muller, M., Dirschinger, J., Schomig, A., 2003. Intracoronary stenting and angiographic results: Strut thickness effect on restenosis outcome (ISAR-STEREO-2) trial. Journal of the American College of Cardiology 41, 1283-1288.

Papafaklis, M.I., Bourantas, C.V., Theodorakis, P.E., Katsouras, C.S., Naka, K.K., Fotiadis, D.I., Michalis, L.K., 2010. The Effect of Shear Stress on Neointimal Response Following Sirolimus-

and Paclitaxel-Eluting Stent Implantation Compared With Bare-Metal Stents in Humans. Journal of the American College of Cardiology-Cardiovascular Interventions 3, 1181-1189.

Peacock, J., Hankins, S., Jones, T., Lutz, R., 1995. Flow instabilities induced by coronary artery stents: assessment with an in vitro pulse duplicator. Journal of biomechanics 28, 17-26.

Räber, L., Juni, P., Loffel, L., Wandel, S., Cook, S., Wenaweser, P., Togni, M., Vogel, R., Seiler, C., Eberli, F., Luscher, T., Meier, B., Windecker, S., 2010. Impact of stent overlap on angiographic and long-term clinical outcome in patients undergoing drug-eluting stent implantation. Journal of the American College of Cardiology 55, 1178-1188.

Rikhtegar, F., Knight, J.A., Olgac, U., Saur, S.C., Poulikakos, D., Marshall, W., Cattin, P.C., Alkadhi, H., Kurtcuoglu, V., 2012. Choosing the optimal wall shear parameter for the prediction of plaque location—A patient-specific computational study in human left coronary arteries. Atherosclerosis 221, 432-437.

Rikhtegar F, P.F., Wyss C, Stok KS, Ge H, Choo RJ, Ferrari A, Poulikakos D, Müller R, Kurtcuoglu V, 2013. Compound Ex Vivo and In Silico Method for Hemodynamic Analysis of Stented Arteries. PLoS One 8, e58147.

Rogers, C., Edelman, E.R., 1995. Endovascular Stent Design Dictates Experimental Restenosis and Thrombosis. Circulation 91, 2995-3001.

Samady, H., Eshtehardi, P., McDaniel, M.C., Suo, J., Dhawan, S.S., Maynard, C., Timmins, L.H., Quyyumi, A.A., Giddens, D.P., 2011. Coronary Artery Wall Shear Stress Is Associated With Progression and Transformation of Atherosclerotic Plaque and Arterial Remodeling in Patients With Coronary Artery Disease. Circulation 124, 779-788.

Serruys, P.W., Foley, D.P., Suttorp, M.J., Rensing, B.J., Suryapranata, H., Materne, P., van den Bos, A., Benit, E., Anzuini, A., Rutsch, W., Legrand, V., Dawkins, K., Cobaugh, M., Bressers, M., Backx, B., Wijns, W., Colombo, A., 2002. A randomized comparison of the value of additional stenting after optimal balloon angioplasty for long coronary lesions: final results of the additional value of NIR stents for treatment of long coronary lesions (ADVANCE) study. Journal of the American College of Cardiology 39, 393-399.

Stone, P.H., Coskun, A.U., Kinlay, S., Clark, M.E., Sonka, M., Wahle, A., Ilegbusi, O.J., Yeghiazarians, Y., Popma, J.J., Orav, J., Kuntz, R.E., Feldman, C.L., 2003. Effect of Endothelial Shear Stress on the Progression of Coronary Artery Disease, Vascular Remodeling, and In-Stent Restenosis in Humans: In Vivo 6-Month Follow-Up Study. Circulation 108, 438-444.

Tsagalou, E., Chieffo, A., Iakovou, I., Ge, L., Sangiorgi, G.M., Corvaja, N., Airoldi, F., Montorfano, M., Michev, I., Colombo, A., 2005. Multiple overlapping drug-eluting stents to treat diffuse disease of the left anterior descending coronary artery. Journal of the American College of Cardiology 45, 1570-1573.

van der Giessen, A.G., Groen, H.C., Doriot, P.-A., de Feyter, P.J., van der Steen, A.F.W., van de Vosse, F.N., Wentzel, J.J., Gijsen, F.J.H., 2011. The influence of boundary conditions on wall shear stress distribution in patients specific coronary trees. Journal of Biomechanics 44, 1089-1095.

van Geuns, R.-J., Tamburino, C., Fajadet, J., Vrolix, M., Witzenbichler, B., Eeckhout, E., Spaulding, C., Reczuch, K., La Manna, A., Spaargaren, R., García-García, H.M., Regar, E., Capodanno, D., Van Langenhove, G., Verheye, S., 2012. Self-Expanding Versus Balloon-Expandable Stents in Acute Myocardial Infarction: Results From the APPOSITION II Study: Self-Expanding Stents in ST-Segment Elevation Myocardial Infarction. Journal of the American College of Cardiology-Cardiovascular Interventions 5, 1209-1219.

Wang, K., Zhou, X.R., Verbeken, E., Ping, Q.B., Huang, Y.M., Huang, J.H., Van de Werf, F., De Scheerder, I., 2000. Overlapping coronary stents result in an increased neointimal hyperplasia: Insight from a porcine coronary stent model. Journal of Interventional Cardiology 13, 173-177.

Wells, D.R., Archie Jr, J.P., Kleinstreuer, C., 1996. Effect of carotid artery geometry on the magnitude and distribution of wall shear stress gradients. Journal of Vascular Surgery 23, 667-678.

Wentzel, J.J., Gijsen, F.J.H., Schuurbiers, J.C.H., van der Steen, A., Serruys, P.W., 2008. The influence of shear stress on in-stent restenosis and thrombosis. EuroIntervention 4, C27-C32.

Wentzel, J.J., Krams, R., Schuurbiers, J.C., Oomen, J.A., Kloet, J., van Der Giessen, W.J., Serruys, P.W., Slager, C.J., 2001. Relationship between neointimal thickness and shear stress after Wallstent implantation in human coronary arteries. Circulation 103, 1740-1745.

Williams, A.R., Koo, B. K., Gundert, T.J., Fitzgerald, P.J., LaDisa, J.F., 2010. Local hemodynamic changes caused by main branch stent implantation and subsequent virtual side branch balloon angioplasty in a representative coronary bifurcation. Journal of Applied Physiology 109, 532-540.

Figures

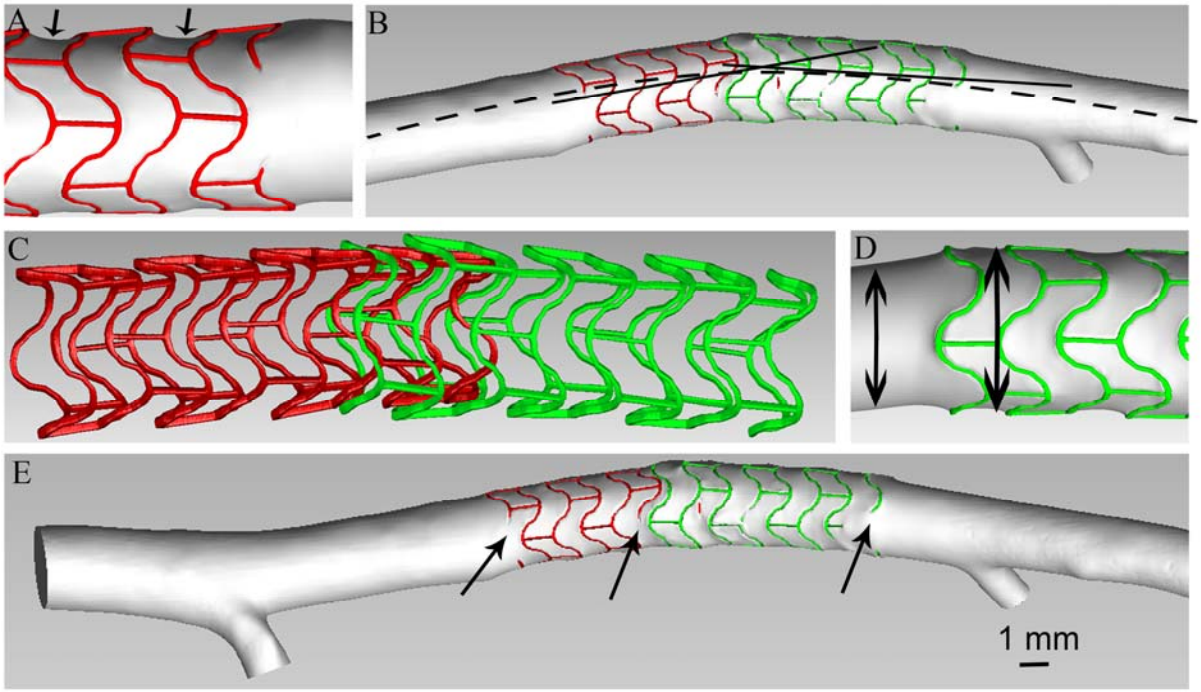

Fig.1. Porcine left coronary artery lumen negative with two overlapping stents. (A) Areas of tissue prolapse (arrows) between stent struts (red). (B) Axial arterial deformation due to stenting. The solid lines show the individual longitudinal axes of the two deployed stents (red and green), while the dashed line approximates the centerline of the stent-free artery. (C) Reconstructed surface of overlapping stents, visualizing relative strut positioning in the region of overlap. (D) Radial arterial deformation caused by stenting. The arrows indicate arterial diameter in the stented (right) and stent-free regions. (E) The embedded stents with the captured lumen negative. Malapposed strut sections are marked by arrows.

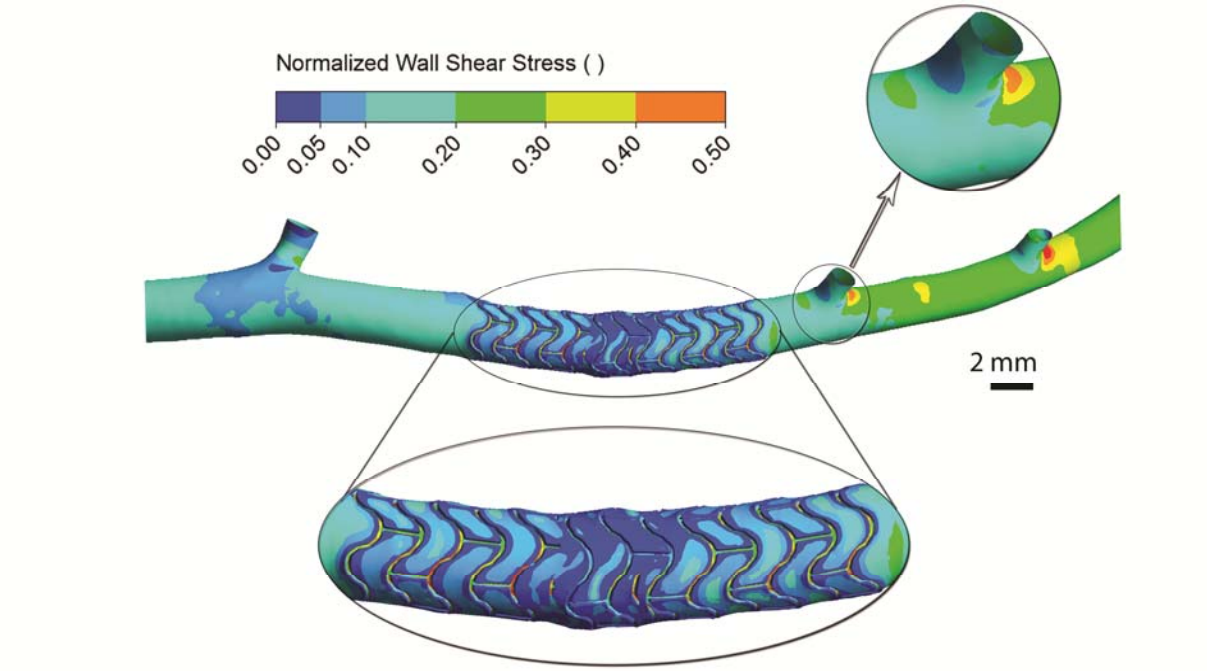

Fig. 2. Normalized wall shear stress distribution in a porcine left coronary artery with two overlapping stents. Magnified views of the stented segment and a bifurcation are shown in the insets. Wall shear stress (WSS) below 5% of maximum WSS occurs mainly in the vicinity of stent struts and at bifurcations, which are sites known to be prone to intimal thickening. A large area of low WSS is observed in the region of stent overlap.

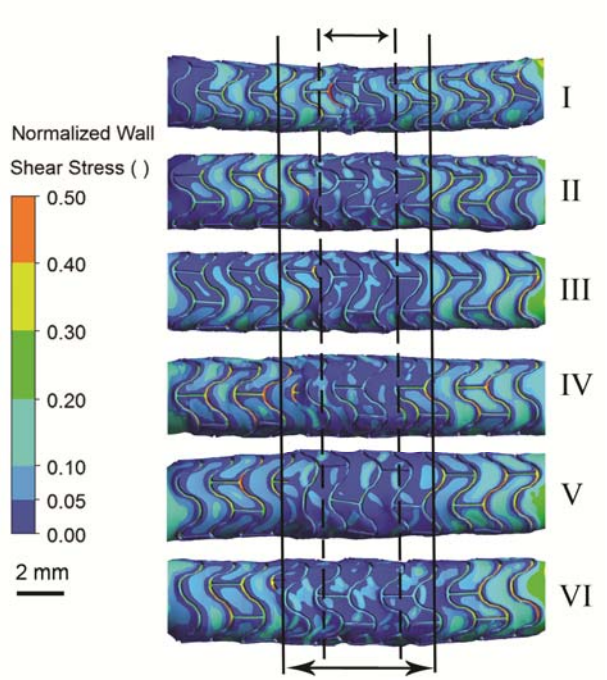

520

521 **Fig. 3. Normalized wall shear stress distribution in the stented segment of six arteries with**
522 **overlapping stents.** Flow direction is from left to right. A large area of low WSS (< 5% of maximum
523 WSS) is clearly visible in all samples. The extent of the low WSS region depends on the number of
524 overlapping struts. The first three cases have shorter length of overlap (two to three struts) compared
525 to the remaining cases (four to five struts). The approximate length of overlap for the first three
526 samples is indicated by the dashed lines, while the approximate borders of the remaining samples are
527 shown with solid lines.

528

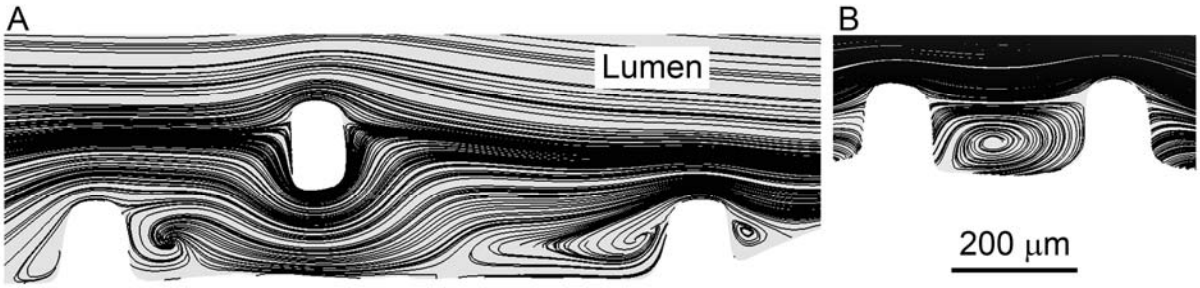

529

530 **Fig. 4. Projection of streamlines to cut plane in the vicinity of stent struts.** (A) Streamlines in

531 overlapping segment with alternating struts. Recirculation zones are clearly visible near the stent

532 struts. (B) Large area of recirculation between two struts in close proximity.

533

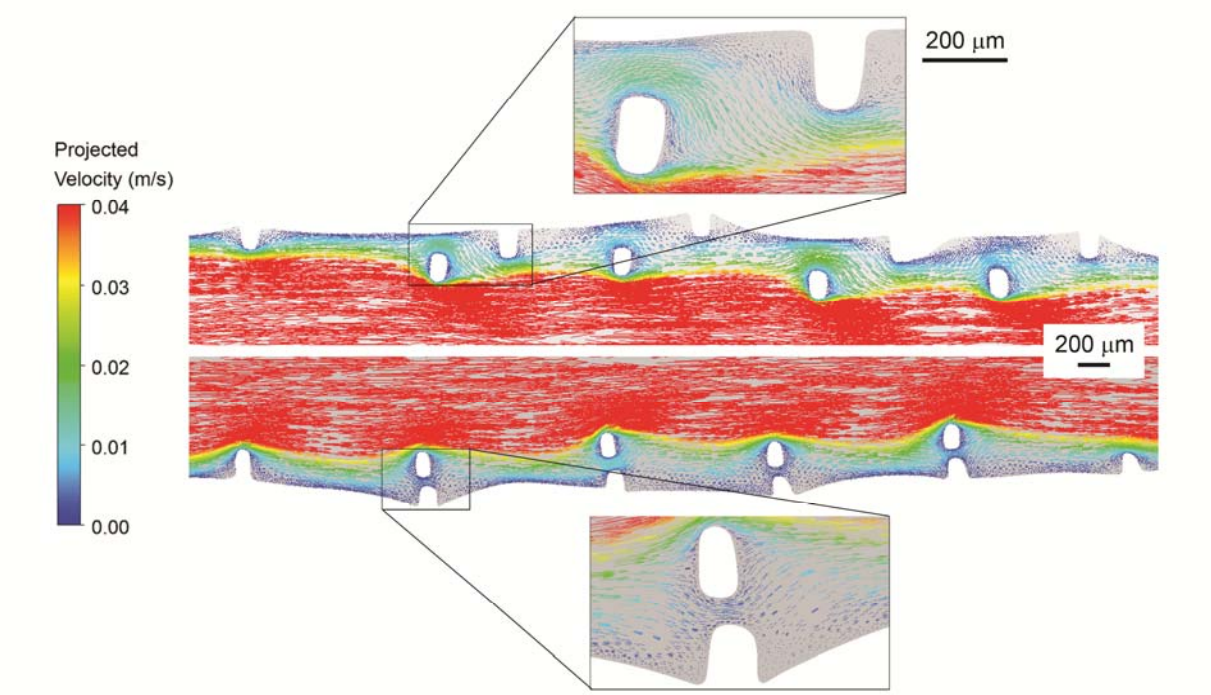

Fig. 5. Vector plots of projected velocity for two different stent overlap configurations. Top panel: Alternating (incongruent) struts. Bottom panel: Aligned (congruent) struts. The latter configuration is associated with lower near-wall velocities (bottom inset) and decreased WSS (compare Fig. 6), while in the former relatively high velocities are maintained in proximity of the wall (top inset).

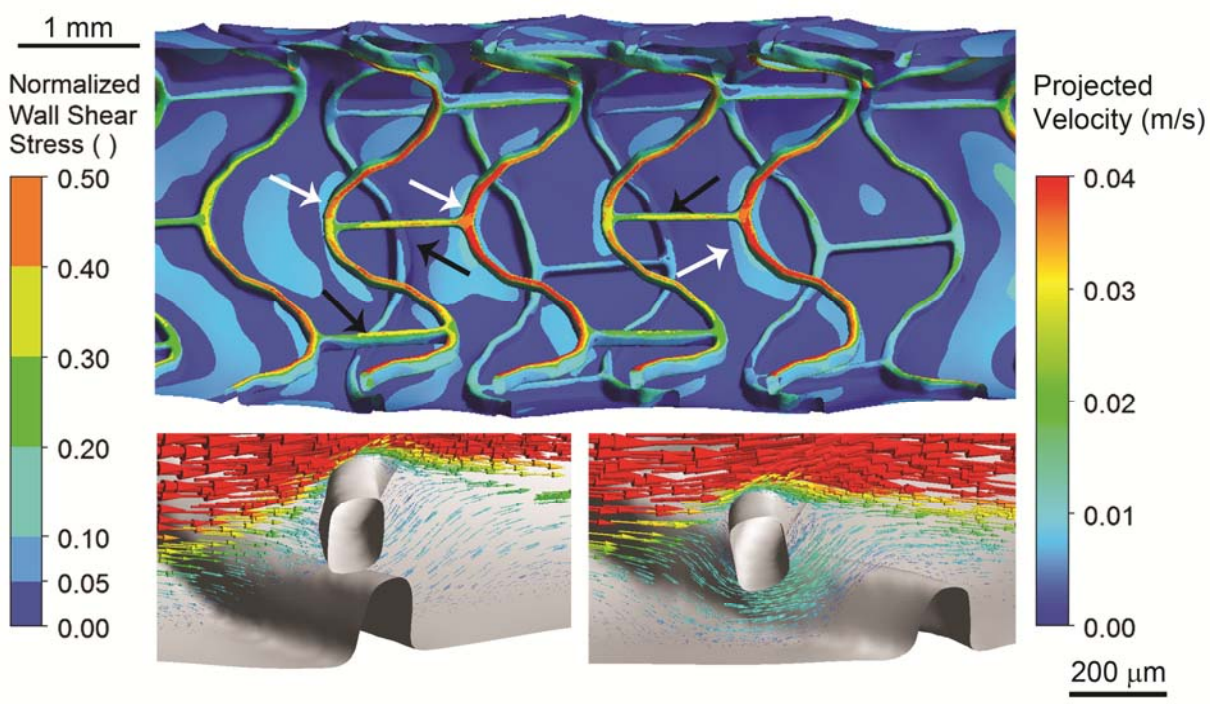

Fig. 6. The effect of strut alignment on wall shear stress and velocity distribution. Top panel: Longitudinal cut through stented artery section. Color map shows normalized shear stress distribution on stent surfaces and artery wall. Low WSS is seen in areas adjacent to congruent struts (black arrows), while higher WSS is observed near incongruent struts (white arrows). Bottom panels: Vector plot of velocities projected onto axial cut plane in the vicinity of congruent (left) and incongruent struts (right).

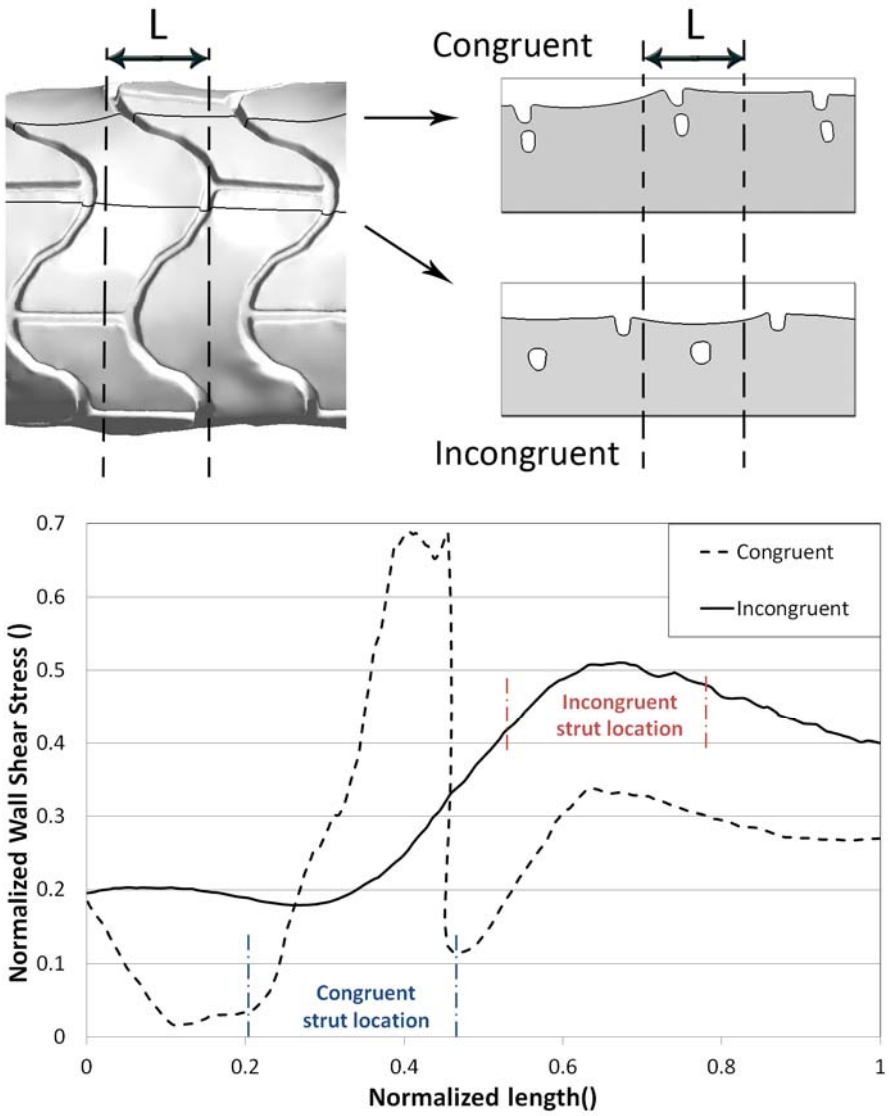

549

550 **Fig. 7. Comparison of normalized wall shear stress near congruent and incongruent struts.** Top
551 left panel: Rendering of the studied arterial segment. Shear stress values plotted in the bottom panel
552 are obtained in the region of length L between the dashed vertical lines. Longitudinal sections shown
553 in the top right panel are obtained along the two solid black lines. Top right panel: Longitudinal cross-
554 sections at congruent and incongruent struts locations according to the rendering in the top left panel.
555 Bottom panel: Normalized WSS plotted versus normalized axial distance from the left to the right
556 dashed vertical lines shown in the top panels. WSS is generally lower for the congruent case due to
557 lower velocity near the wall, with the exception of the actual strut pair location. There, flow is
558 tunneled between the closely spaced struts, leading to high WSS.

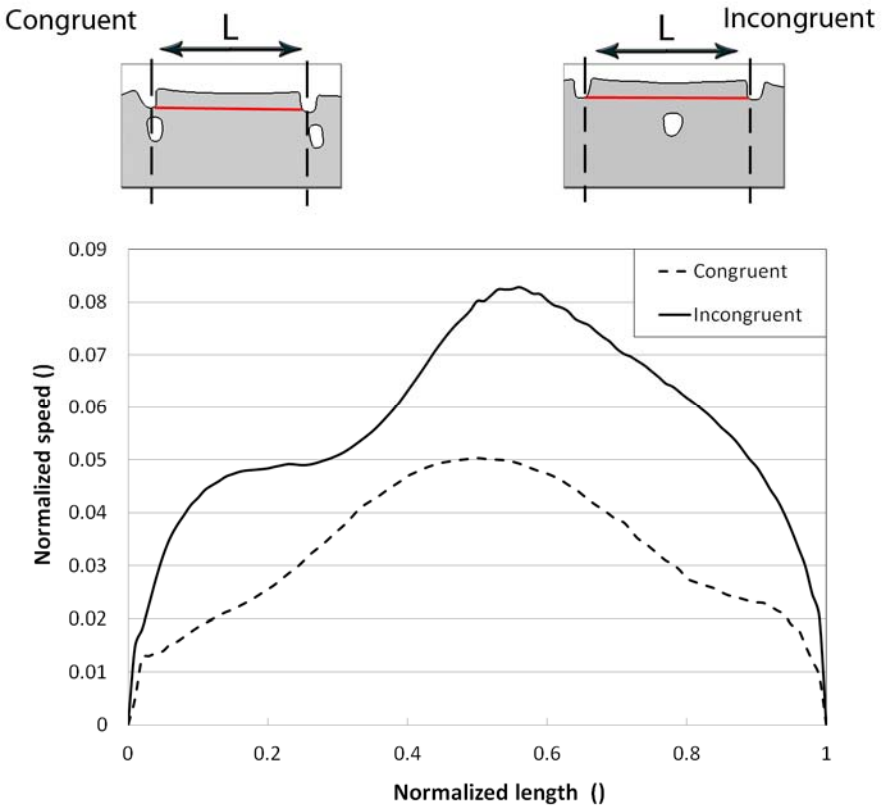

559

560 **Fig. 8. Normalized velocity between adjacent struts in congruent and incongruent**
561 **configurations.** Bottom panel: Blood flow velocity magnitude along red path shown in the top panels
562 for the strut configurations shown in the top panels. Velocities are normalized by the respective
563 values at the same longitudinal position on the arterial centerline. The horizontal axis shows distance
564 from the left endpoint of the red path normalized by the length L of that path. In the congruent case,
565 the collocation of the struts forms a taller obstacle to blood flow, resulting in a larger recirculation area
566 and reduced velocity between the adjacent strut pairs.

567

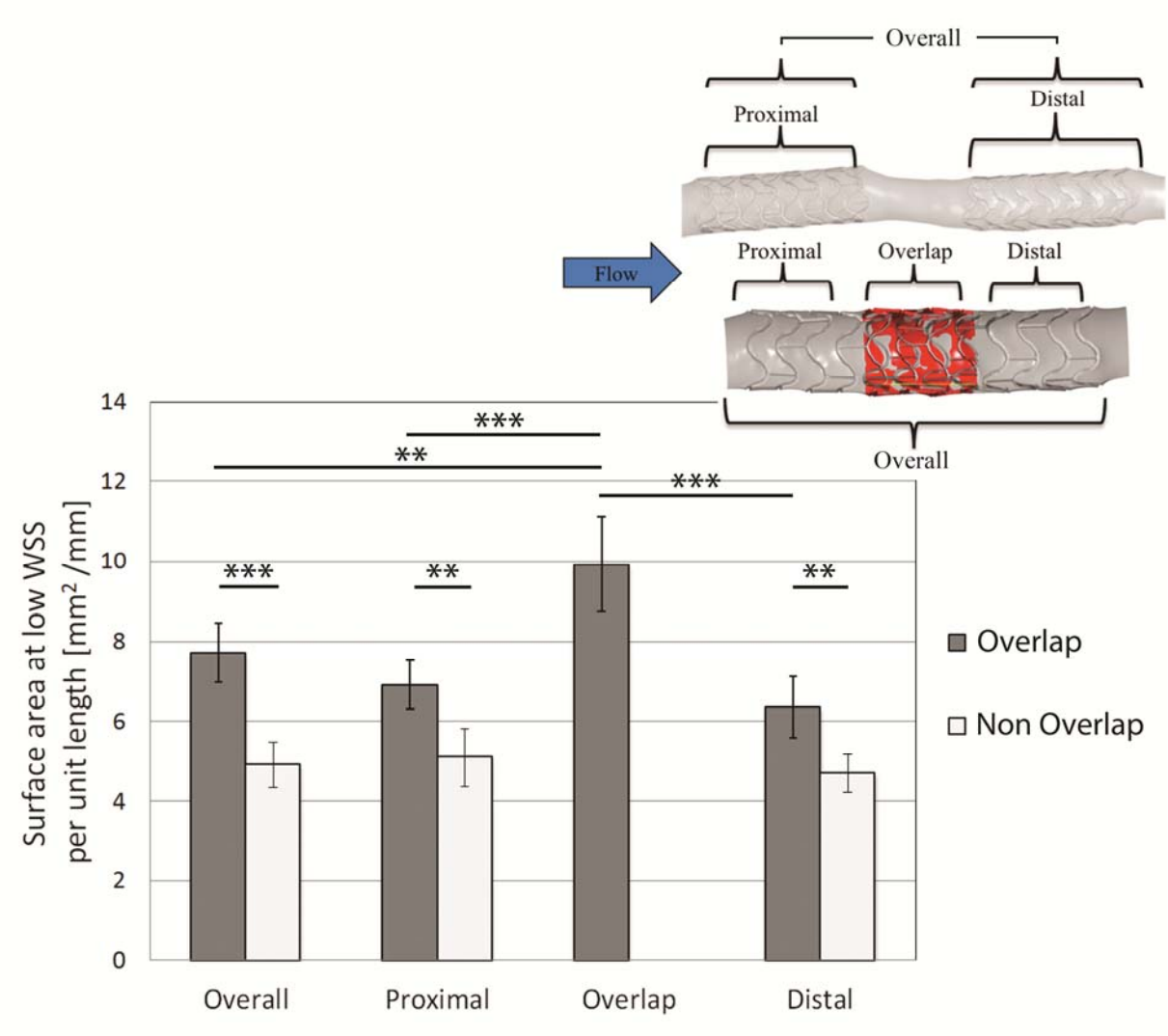

Fig. 9. Comparison of relative artery wall area exposed to low WSS in different segments of overlapping and non-overlapping stents. The bar height (mean value over all investigated cases) indicates wall surface area per unit length exposed to WSS below 5% of maximum WSS in arteries with overlapping stents (dark) and non-overlapping stents (light). Values are given for each segment as defined in the inset. Error bars indicate the standard error. Significant differences between the sample means according to unpaired t-test are indicated by asterisks (** for $p < 0.01$, *** for $p < 0.001$). The overlap region shows a substantially larger area of low WSS not only compared to the non-overlap cases, but also compared to the segments proximal and distal of the overlap segment.